Journal of Materials Chemistry B

PAPER

View Article Online
View Journal | View Issue

Cite this: J. Mater. Chem. B, 2019, 7, 7326

Medical fluorophore 1 (MF1), a benzoquinolizinium-based fluorescent dye, as an inflammation imaging agent†

Sang Bong Lee,‡[a] Ye Ri Han,‡[a] Hui-Jeon Jeon,‡[a] Chul-Ho Jun,[bcd] Sang-Kyoon Kim,[e] Jungwook Chin,[a] Su-Jeong Lee,[a] Minseon Jeong,[a] Jae-Eon Lee,[ef] Chang-Hee Lee,[bcd] Sung Jin Cho,*[a] Dong-Su Kim*[a] and Yong Hyun Jeon*[e]

Received 24th June 2019,
Accepted 14th October 2019

DOI: 10.1039/c9tb01266d

rsc.li/materials-b

Structure-based targeting of fluorescent dyes is essential for their use as imaging agents for disease diagnosis. Here, we describe the development of the benzoquinolizinium compound Medical fluorophore 1 (MF1) as a novel biomedical imaging agent that allows the visualization of inflammation by virtue of its unique chemical structure. Lipopolysaccharide treatment stimulated the uptake of MF1 by bone marrow-derived macrophages, with no adverse effects on cell proliferation. *In vivo* fluorescence lifetime imaging revealed the accumulation of MF1 in carrageenan-induced acute inflammatory lesions in mice, which peaked at 6 h. MF1-based imaging also allowed monitoring of the response to the anti-inflammatory drugs dexamethasone and sulfasalazine. Thus, MF1 can be used to diagnose diseases characterized by inflammation as well as treatment efficacy.

Introduction

Inflammation is an innate and adaptive immune response induced by infectious pathogens such as bacteria, viruses, and fungi[1–3] as well as noxious stimuli and conditions such as tissue injury[4,5] and degeneration, cell death,[6–8] cancer,[9] ischemia,[10] and thrombosis.[11,12] Inflammation provides a mechanism for removing irritants and restoring tissue homeostasis. Immune activation involves inflammation mediated by white blood cells,[13] followed by stimulation of T lymphocytes[14] that results in the activation of monocytes,[15] mast cells,[16,17] dendritic cells,[18,19] and macrophages.[20,21] An inadequate immune response can lead to chronic disease; monitoring inflammation can provide insights into pathophysiological states.

Near-infrared (NIR) fluorophores have many desirable characteristics for medical imaging purposes including low tissue attenuation, low autofluorescence, and ability to penetrate into deep tissue.[22,23] NIR fluorophores with covalently bound small molecules,[24,25] peptidomimetics,[26,27] peptides,[28,29] nanostructures,[30,31] and antibodies[32,33] that can be targeted to specific tissues have been developed.[34–41] However, despite their advantages the high molecular weight of modified fluorophores and their complex routes of synthesis limit their widespread application.

We recently reported the development of several novel fluorescent dyes using a unique synthesis approach based on benzoquinolizinium salts.[42] One of these dyes, Medical fluorophore 1 (MF1), is an attractive probe for *in vivo* imaging owing to its facile synthesis, long wavelength and Stokes shift, and biocompatibility.

Herein we demonstrate the utility of MF1 for visualizing inflammatory lesions *in vivo* by optical imaging (Fig. 1) and for evaluating the physiological response to anti-inflammatory drugs.

Experimental section

General

^{1}H Nuclear magnetic resonance (NMR) and ^{13}C NMR spectra were recorded on an Avance II/DPX 400 (400 MHz ^{1}H, 100 MHz ^{13}C) spectrometer (Bruker, Billerica, MA, USA) with chemical shifts reported relative to residual deuterated solvent peaks.

[a] New Drug Development Center, Daegu-Gyeongbuk Medical Innovation Foundation, 80 Chembok-ro Dong-gu Daegu, Republic of Korea. E-mail: dongsukim1127@dgmif.re.kr, sjcho@dgmif.re.kr
[b] Department of Chemistry, Yonsei University, 50 Yonsei-ro, Seodaemun-gu, Seoul 03722, Republic of Korea
[c] Center for NanoMedicine, Institute for Basic Science (IBS), Seoul, Republic of Korea
[d] Yonsei-IBS Institute, Yonsei University, Seoul 03722, Republic of Korea
[e] Laboratory Animal Center, Daegu-Gyeongbuk Medical Innovation Foundation, 80 Chembok-ro Dong-gu Daegu, Republic of Korea. E-mail: jeon9014@gmail.com
[f] Department of Biomaterials Science, College of Natural Resources and Life Science/Life and Industry Convergence Research Institute, Pusan National University, Pusan, Republic of Korea

† Electronic supplementary information (ESI) available. See DOI: 10.1039/c9tb01266d

‡ These authors contributed equally.

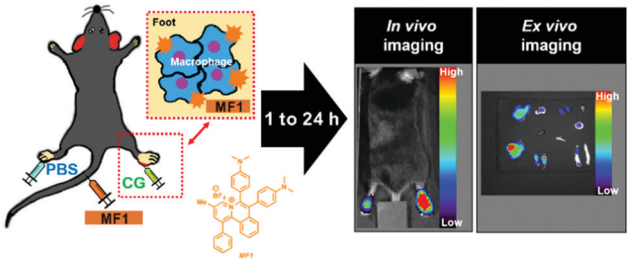

Fig. 1 *In vivo* FLI of acute inflammation with MF1. The dye was intravenously injected into mice with carrageenan (CG)-induced inflammation, followed by *in vivo* fluorescence imaging. Red dotted squares show region of acute inflammation.

Infrared spectra were obtained using a Nicolet Impact 400 spectrometer (Thermo Fisher Scientific, Waltham, MA, USA). ^{1}H NMR spectra are reported as follows: chemical shift, multiplicity (s = singlet, d = doublet, t = triplet, q = quartet, m = multiplet, dd = doublet of doublet, ddd = doublet of doublet of doublet). ^{13}C NMR spectra were referenced to the residual $CDCl_3$ (77.26 ppm) and MeOD-d_4 (47.59 ppm). Mass spectra were obtained in positive electrospray ionization (ESI) mode on an LCMS-2020 system (Shimadzu, Tokyo, Japan). Column chromatography was performed using a CombiFlash Rf system with RediSep Rf (Teledyne Isco, Lincoln, NE, USA). The final compounds were purified by preparative high-performance liquid chromatography (HPLC) on a Kinetex 5 μm biphenyl 100 Å GX-281 HPLC system (Gilson, Middleton, WI, USA; column tube 250 × 21.2 mm inner diameter), with ACN/H_2O as eluent. The purity of compounds was evaluated by analytical HPLC using a dual-wavelength ultraviolet detector. Fluorescence data were recorded on an F-4500 spectrophotometer (Hitachi, Tokyo, Japan). High resolution mass spectra (HRMS) were acquired on a 1290 Infinity LC/6530 Accurate-Mass Q-TOF system (Agilent Technologies, Santa Clara, CA, USA) at Yonsei Center for Research Facilities, Yonsei University. Commercially available reagent-grade chemicals were used as received without further purification unless otherwise stated. $[Cp^*RhCl_2]_2$[43] and functionalized internal alkynes[44,45] were prepared as previously described.

Chemistry

Synthesis of 5-methyl-2,3-diphenylpyridine (4a; CAS No. 122801-45-0). 2-Methyl-*N*-phenethylprop-2-en-1-amine (**1a**; 0.2 mmol), diphenylacetylene (**2a**; 0.4 mmol), $Cu(OAc)_2$ (0.4 mmol), $[Cp^*RhCl_2]_2$ (5 mol%), HBF_4 (48% in water, 0.3 mmol), and methanol were added to a 1 ml pressure vial. The solution was stirred at 130 °C for 6 h, dried over anhydrous $MgSO_4$, and filtered; the filtrate was concentrated *in vacuo*. Pyridinium salt 5-methyl-1-phenethyl-2,3-diphenylpyridin-1-ium tetrafluoroborate (**3a**) was obtained by column chromatography (DCM : MeOH = 1 : 1) with a 84% yield (white solid, 71.1 mg). The melting point was 154–156 °C. The NMR data are as follows: ^{1}H NMR (400 MHz, $CDCl_3$) δ 8.84 (s, 1H), 8.09 (s, 1H), 7.40 (t, J = 7.6 Hz, 1H), 7.32 (t, J = 7.6 Hz, 2H), 7.19–7.12 (m, 8H), 7.05–7.04 (m, 2H), 6.81–6.79 (m, 2H), 4.62 (t, J = 7.6 Hz, 2H), 3.05 (t, J = 8.0 Hz, 2H), 2.57 (s, 3H); ^{13}C NMR (100 MHz, $CDCl_3$) δ 151.3, 146.8, 145.0, 142.6, 138.7, 135.5, 135.4, 130.8, 130.09, 130.04, 129.4, 129.2, 129.0, 128.8, 128.7, 128.6, 127.5, 60.7, 37.2, 18.4.

5-Methyl-1-phenethyl-2,3-diphenylpyridin-1-ium tetrafluoroborate (**3a**; 2 mmol), C_2H_5ONa (5 eq.), and methanol were added to a 5 ml pressure vial. The solution was stirred at 130 °C for 6 h and filtered; the filtrate was concentrated *in vacuo*. 5-Methyl-2,3-diphenylpyridine (**4a**) was obtained by column chromatography (Hex : EA = 5 : 1) with a 78% yield (white solid, 382.7 mg). The NMR data are as follows: ^{1}H NMR (400 MHz, $CDCl_3$) δ 8.54 (d, J = 1.6 Hz, 1H), 7.55 (d, J = 1.2 Hz, 1H), 7.37–7.34 (m, 2H), 7.28–7.25 (m, 3H), 7.24–7.23 (m, 3H), 7.20–7.17 (m, 2H), 2.43 (s, 3H); ^{13}C NMR (100 MHz, $CDCl_3$) δ 154.3, 148.7, 140.0, 139.8, 138.9, 135.3, 131.4, 129.7, 129.4, 128.1, 127.7, 127.4, 127.0, 17.8.

Synthesis of 3-methyl-1-phenyl-6,7-dipropylpyrido[2,1-*a*]-isoquinolin-5-ium tetrafluoroborate (6a; MF1). 5-Methyl-2,3-diphenylpyridine (**4a**; 0.2 mmol), 4,4′-(ethyne-1,2-diyl)bis(*N*,*N*-dimethylaniline) (**5a**; 0.4 mmol), $Cu(OAc)_2$ (0.4 mmol), $[Cp^*RhCl_2]_2$ (5 mol%), $NaBF_4$ (0.3 mmol), and methanol were added to a 1 ml pressure vial. The solution was stirred at 130 °C for 6 h, dried over anhydrous $MgSO_4$, and filtered; the filtrate was concentrated *in vacuo*. 6,7-Bis(4-(dimethylamino)phenyl)-3-methyl-1-phenylpyrido-[2,1-*a*]isoquinolin-5-ium tetrafluoroborate was obtained by preparative HPLC (ACN:H_2O) with a 99% yield (**6a**, MF1; brown solid, 117.9 mg). The NMR data are as follows: ^{1}H NMR (400 MHz, MeOD-d_4) δ 8.79 (s,1H), 8.39 (s, 1H), 8.02 (d, J = 8.6 Hz, 1H), 7.77 (t, J = 7.7 Hz, 1H), 7.66–7.58 (m, 6H), 7.40 (t, J = 7.9 Hz, 1H), 7.34 (d, J = 8.5 Hz, 2H), 7.25 (q, J = 8.6 Hz, 4H), 6.87 (d, J = 8.7 Hz, 2H), 3.15 (s, 6H), 3.04 (s, 6H), 2.55 (s, 3H); ^{13}C NMR (100 MHz, MeOD-d_4) δ 150.8, 146.4, 144.1, 141.9, 140.1, 139.8, 139.4, 136.2, 134.5, 133.8, 133.6, 132.5, 131.7, 131.5, 129.8, 129.4, 129.2, 128.5, 127.8, 126.7, 124.7, 118.5, 115.9, 112.5, 42.2, 39.0, 17.0; IR (neat): 2919, 2803, 1658, 1609, 1431, 1059 (ν_{B-F}), 1029, 817, 730 cm^{-1}; HRMS (ESI) calculated for $C_{36}H_{34}N_3^+$ 508.2747, found 508.2744.

Animals

Specific pathogen-free immunocompetent 6-week old C57BL/6 mice were obtained from Japan SLC (Shizuoka, Japan). All experimental procedures involving animals were conducted in strict accordance with the international guidelines for animal research. The study protocol was approved by the Committee on the Ethics of Animal Experiments of the Laboratory Animal Center of Daegu-Gyeongbuk Medical Innovation Foundation (approval no. DGMIF-18070202-00).

Cells

BJ normal human fibroblasts were grown in custom Dulbecco's modified Eagle's medium (Hyclone, Logan, UT, USA) supplemented with 10% fetal bovine serum (FBS; Hyclone) and 1% penicillin–streptomycin (Gibco, Grand Island, NY, USA). Mouse bone marrow-derived macrophages (BMDMs) were obtained from the tibia and femur of C57BL/6 mice. Briefly, bone marrow cells were cultured in α-Minimal Essential Medium containing 10% FBS and 30% L929 cell-conditioned medium for 7 days. The medium was changed every 2–3 days. BMDMs were then seeded for subsequent experiments.

Cell proliferation assay

Cell proliferation was evaluated using Cell Counting Kit 8 (CCK-8; Dojindo Laboratories, Tokyo, Japan). BJ cells and BMDMs were seeded at 1×10^4 cells per well in 96-well plates, and 10 μl of CCK-8 solution were added to each well after 24 h of incubation with MF1 at a concentration of 10–25 μM, followed by incubation at 37 °C for 1 h. Absorbance at 450 nm was measured on a microplate reader (BMG Labtech, Offenburg, Germany).

Cytokine analysis

The culture supernatant of unlabeled or MF1-labeled BMDMs was collected and analyzed for IL-1β, TNF-α, and IL-6 levels using commercially available cytokine enzyme-linked immunosorbent assay kits (R&D Systems, Minneapolis, MN, USA).

Immunofluorescence confocal microscopy

BMDMs were treated MF1 and lipopolysaccharide (100 ng mL^{-1}) for 24 h and then seeded on coverslips. The cells were washed three times with phosphate-buffered saline (PBS) and fixed overnight at 4 °C with 1% paraformaldehyde (Sigma-Aldrich, St Louis, MO, USA). The cells were rinsed with PBS and permeabilized with 0.1% Triton X-100 in PBS for 10 min at room temperature, then blocked for 1 h with 10% normal goat serum in PBS. Nuclei were stained with 4′,6-diamidino-2-phenylindole (Vector Laboratories, Burlingame, CA, USA). The samples were mounted and visualized with a confocal laser scanning microscope (LSM 800; Carl Zeiss, Oberkochen, Germany). Fluorescence intensity was quantified using ImageJ software (National Institutes of Health, Bethesda, MD, USA).

Animal studies

Study 1. The scheme for imaging acute inflammation *in vivo* is shown in Fig. S7 (ESI†). Briefly, PBS and 1% carrageenan (CG) solution were administered to separate foot pads of each immunocompetent mouse. At 10 min after injection, MF1 (5 mg kg^{-1}) was intravenously administered followed by imaging using an IVIS Spectrum system (PerkinElmer, Waltham, MA, USA) at indicated times.

Study 2. The scheme for drug treatment is shown in Fig. S9 (ESI†). Mice were divided into vehicle, dexamethasone (DEX), and sulfasalazine (SSZ) groups (n = 6 each). Inflammation was induced as described above, and a single dose of 10 mg kg^{-1} DEX, SSZ, or vehicle was administered to the mice immediately afterward. Imaging was performed to visualize MF1 uptake in footpads at indicate times. After image acquisition, the organs were removed for *ex vivo* imaging.

Phenotype marker analysis

PBS and 1% CG were subcutaneously injected into the left and right paws, respectively, of each mouse. At 10 min after injection, MF1 was intravenously administered, and this was followed by a FACS analysis at 6 h. The PBS- and CG-injected paws of mice that were administered MF1 were stained with F4/80 antibody (BD Bio science) at 4 °C for 30 min. The washed macrophage cells were analyzed using flow cytometry. The data were analyzed using FlowJo analysis software (FlowJo, Ashland, OR, USA).

Measurement of 1% CG-induced paw edema

PBS and 1% CG were subcutaneously injected into the left and right paws, respectively, of each mouse. Immediately afterward, the mice were injected with a single dose of 10 mg kg^{-1} DEX, SSZ, or vehicle. Paw edema was measured before (0 h, baseline) and 3, 6, and 24 h after induction of inflammation. The change in dorsoventral thickness of the middle portions of the injected paws was measured using calipers as previously described.[46]

In vivo fluorescence imaging

In vivo fluorescence images were acquired using an IVIS Lumina III imaging system (PerkinElmer). The scan times ranged from 1 s to 5 min depending on the intensity of the emitted fluorescence signal. The image was thresholded to maximize visualization of the region of interest and minimize background fluorescence. Grayscale and fluorescence color images were superimposed using LIVINGIMAGE v.2.12 (PerkinElmer) and IGOR Image Analysis FX (Wave Metrics, Lake Oswego, OR, USA) software. Signal intensity is expressed in units of photons per cm^2 per second per steradian (P cm^{-2} s^{-2} sr^{-1}).

Statistical analysis

Data are expressed as mean ± standard deviation of at least three independent experiments. The statistical significance of mean differences was evaluated with the unpaired Student's t test using Prism v.5 software (GraphPad, La Jolla, CA, USA). P values < 0.05 were considered statistically significant.

Results and discussion

Synthesis and characterization of MF1

We synthesized an NIR fluorophore that can be prepared *via* a simple organometallic reaction catalyzed by rhodium(III) (Fig. 2a). Briefly, the reaction of 2-methyl-*N*-phenethylprop-2-en-1-amine (**1a**) with diphenyl acetylene (**2a**) and aqueous HBF_4 in the presence of $(Cp^*RhCl_2)_2$ and $Cu(OAc)_2$ forms pyridinium salt (**3a**) that reacts with NaOEt in MeOH to produce **4a**, with a yield of 78%. Rh(III) catalyzes the *N*-annulation of **4a** with 4,4′-(ethyne-1,2-diyl)bis(*N*,*N*-dimethylaniline) providing benzoquinolizinium salt (**6a**, MF1), which was confirmed by ^1H and ^{13}C nuclear magnetic resonance, liquid chromatography-mass spectrometry, and high-performance liquid chromatography (Fig. S1–S3, ESI†). The synthesized MF1 had excitation/emission wavelengths of 470/688 nm and a long Stokes shift at 218 nm (Fig. 2b). In addition, the full optical characterization data of MF1 are shown in ESI† (Table S1). *In vitro* fluorescence lifetime imaging (FLI) revealed a dose-dependent increase in the fluorescence signal in the MF1-containing tube (Fig. 2c), implying that MF1 has optical properties that are suitable for *in vivo* imaging.

Cell imaging and biological functional assay

For successful *in vivo* application, an imaging agent should not induce toxicity. We therefore examined the effects of MF1 on the viability of normal fibroblasts (BJ) and bone marrow-derived macrophages (BMDMs) and on cytokine secretion.

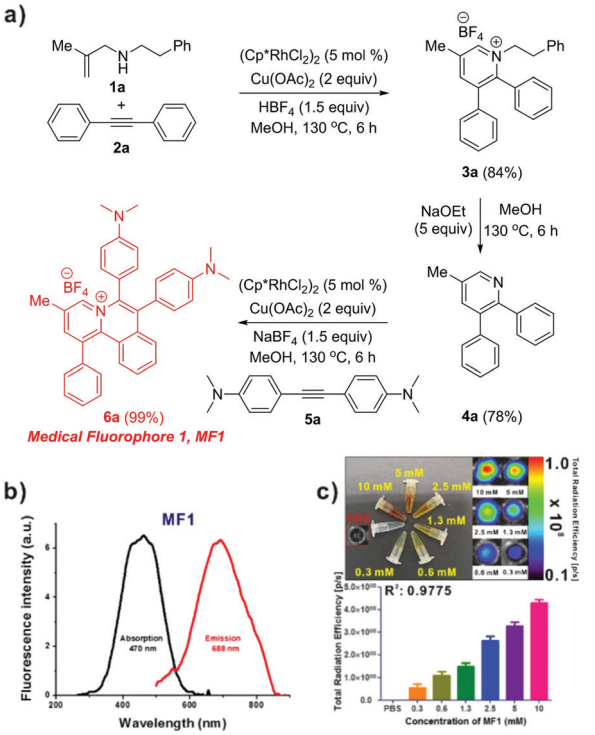

Fig. 2 Route of synthesis and optical properties of MF1. (a) Scheme of MF1 synthesis. (b) Fluorescence spectrum of MF1. (c) *In vitro* FLI signals in tubes containing various concentrations of MF1 (upper: *in vitro* FLI image; bottom: quantification of FLI signal).

As shown in Fig. S4 (ESI†), there were no differences in viability between untreated and treated cells at various doses of MF1. Moreover, the levels of the proinflammatory cytokines tumor necrosis factor α, interleukin 6 (IL-6), and IL-1β did not differ between unlabeled and labeled BMDMs, indicating that MF1 has excellent biocompatibility (Fig. S5, ESI†).

We next evaluated the potential of MF1 as an inflammation-specific imaging agent in BMDMs, which are important effectors in inflammatory lesions. Intact and lipopolysaccharide (LPS)-induced BMDMs were incubated with MF1, and then assessed by confocal fluorescence microscopy analysis. Intact BMDMs showed MF1 accumulation in the cytoplasm but not in the nucleus or plasma membrane (Fig. 3a). Cellular uptake of MF1 was four-fold higher in LPS-induced BMDMs as compared to that in intact BMDMs (Fig. 3b). However, there was no uptake in normal fibroblasts, such as 3TC-L1 and L929 cells (Fig. S6a and b, ESI†). These data indicate that MF1 is selectively taken up by activated but not intact macrophages.

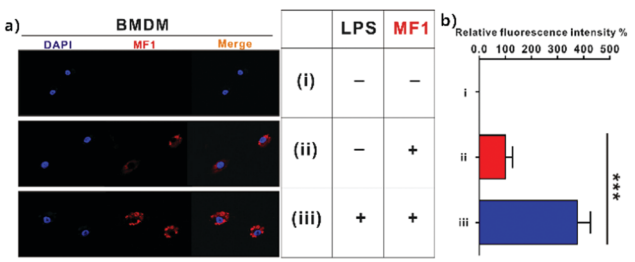

Fig. 3 Uptake of MF1 by BMDMs. (a) Confocal laser scanning microscopy (CLSM) images of BMDMs incubated with MF1 at 37 °C for 1 h. Blue, 4′,6-diamidino-2-phenylindole (DAPI); red, MF1. (b) Quantification of CLSM signals from panel a. Experiments were performed at least in triplicate and values represent mean ± SD. ***$P < 0.001$.

Visualization of MF1 uptake in acute inflammation sites by *in vivo* fluorescence imaging

We next performed *in vivo* fluorescence imaging to assess the potential for MF1 for detecting inflammatory lesions (Fig. S7, ESI†) using a mouse model of carrageenan (CG)-induced acute inflammation.[47] At 3 h after induction of inflammation, MF1 accumulation was observed in the CG-injected paw, with a peak signal intensity at 6 h (Fig. 4a, b and d). There were no significant differences in FLI signal intensity between phosphate-buffered saline- and CG-injected paws at 24 h. Consistent with the *in vivo* FLI results, measurement of dorsoventral thickness of the middle portions of hind paws revealed maximal swelling in CG-injected paws at 6 h, with severe paw edema persisting up to 24 h (Fig. 4c and e). Because the highest uptake was observed in paw edema at 6 h post-injection of MF1, the PBS-injected and CG-injected paws were excised for FACS analysis to examine the percentage of F4/80+ (active macrophage specific marker) and

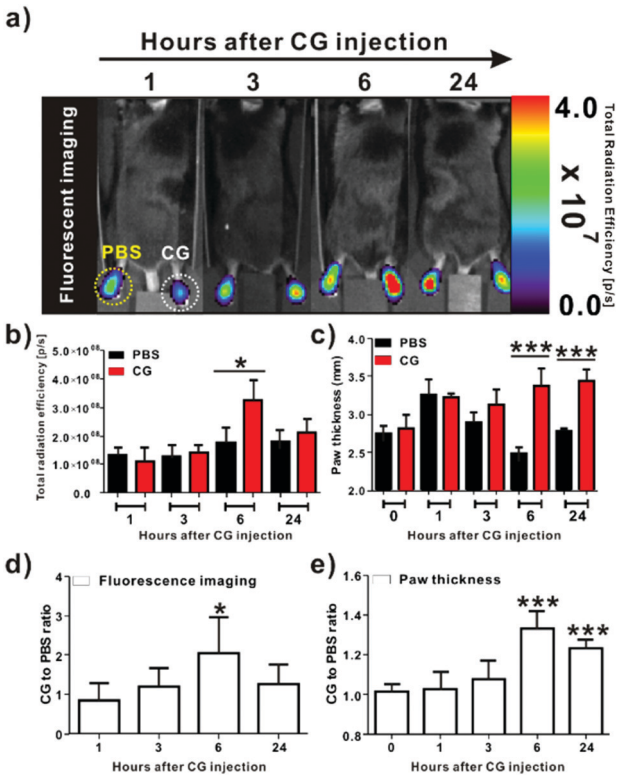

Fig. 4 *In vivo* visualization of an acute inflammatory lesion using MF1. (a) *In vivo* imaging of selective MF1 uptake in inflamed lesions over time. Yellow and white dotted circles indicate phosphate-buffered saline (PBS)- and CG-injected paws, respectively. (b) Region of interest analysis for quantification of fluorescence signal in paws. (c) Measurement of paw thickness. (d) MF1 uptake ratio of CG- to PBS-injected paws. (e) Paw thickness ratio of CG- to PBS-injected footpads. *$P < 0.05$, ***$P < 0.001$.

MF1+ cells. As shown in Fig. S8 (ESI†), the F4/80+ and MF1+ cells were 7.98-fold higher in the CG-injected paw than in the PBS-injected paw. These results indicate that MF1 can be used for *in vivo* monitoring of acute inflammation.

Assessment of the effects of anti-inflammatory agents on MF1 uptake in inflammatory lesions using established inflammation-tracking strategies

We investigated whether imaging inflammation with MF1 can provide a means of evaluating physiological response to anti-inflammatory drugs (Fig. S9, ESI†). We tested this in mice using the anti-inflammatory drugs dexamethasone (DEX; a steroidal drug) and sulfasalazine (SSZ; an antagonist of adenosine A_{2A} cell-surface receptors).

To assess the therapeutic efficacy of DEX and SSZ in CG-induced acute inflammation, immunocompetent mice were injected with the drugs immediately after inducing acute inflammation with CG, followed by intravenous injection of MF1. As shown in Fig. 5, *in vivo* FLI revealed significant inhibition of MF1 uptake in the CG-injected paw of DEX- and SSZ-treated mice 6 h after induction of inflammation (Fig. 5a–c). In contrast, MF1 accumulation was observed in the CG-injected paw of vehicle-treated mice. A measurement of paw thickness showed significant inhibition of paw edema in DEX- or SSZ-treated but not vehicle-treated mice at 6 h post-CG injection (Fig. S10, ESI†).

In *ex vivo* imaging experiments, significant MF1 uptake was evident in the CG-injected paw of vehicle-treated but not DEX- and SSZ-treated mice (Fig. 6). MF1 was also detected in liver, lung, intestine, stomach, spleen, and brain. Thus, MF1-based inflammation imaging is useful for evaluating the physiological response to anti-inflammatory drugs in living organisms.

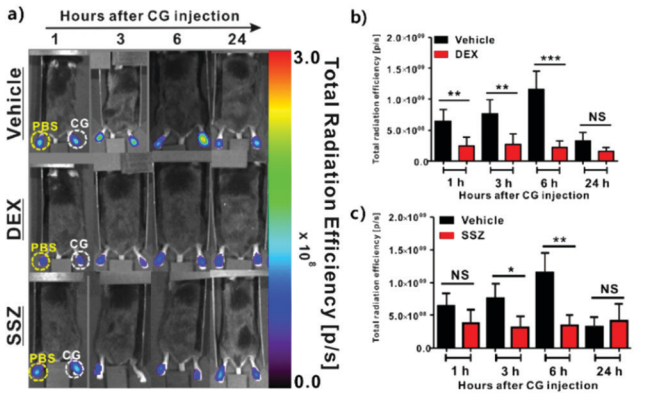

Fig. 5 Assessment of physiological response to anti-inflammation drugs by MF1-based imaging. (a) *In vivo* fluorescence image showing different MF1 uptake levels in vehicle-, DEX-, and SSZ-treated mice. (b) and (c) Quantification of FLI signals from panel (a) (n = 6 per group). Yellow and white circles indicate phosphate-buffered saline (PBS)- and CG-injected paws, respectively. *$P < 0.05$, **$P < 0.01$, ***$P < 0.001$; NS, not significant.

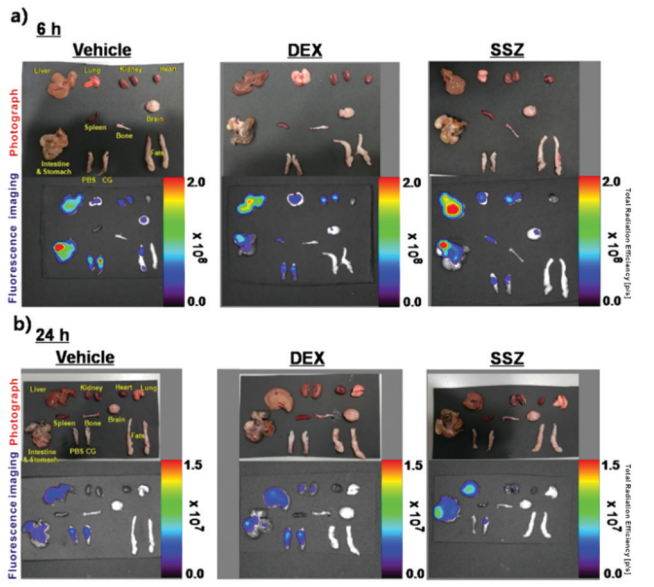

Fig. 6 *Ex vivo* imaging of organs and limbs using MF1. (a and b) Organs including liver, lung, kidney, heart, intestine, stomach, spleen, bone, brain, and fat as well as PBS- or CG-injected paws were visualized at 6 h (a) and 24 h (b) after induction of inflammation.

Conclusions

In conclusion, we demonstrated the specific uptake of the benzoquinolizinium-based MF1 bioimaging agent in LPS-induced BMDMs with no adverse effects of cell proliferation. Importantly, CG-induced inflammatory lesions in immunocompetent mice and the anti-inflammatory effects of SSZ and DEX were successfully visualized by MF1-based imaging, highlighting the utility of MF1 for medical diagnostics. Studies are currently underway to explore other potential applications for this MF1-based imaging platform in cancer, rheumatism, and vascular disease.

Conflicts of interest

There are no conflicts to declare.

Acknowledgements

This work was financially supported by the HI16C1501, HT16C0001, 2017R1D1A1B03028340, 2012M2A2A7013480, 2017R1D1A1B03030196, 2018R1D1AB07047417, NRF-2017R1C1B1005599, 2017M3A9G7073088, 2019R1F1A1057906 and KDDF-201612-16.

References

1 B. Levine, N. Mizushima and H. W. Virgin, *Nature*, 2011, **469**, 323.
2 L. Romani, T. Zelante, A. De Luca, F. Fallarino and P. Puccetti, *J. Immunol.*, 2008, **180**, 5157–5162.
3 M. Monshouwer and K. H. Hoebe, *Toxicol. In Vitro*, 2003, **17**, 681–686.
4 R. a. Dubner and M. Ruda, *Trends Neurosci.*, 1992, **15**, 96–103.
5 M. Mittal, M. R. Siddiqui, K. Tran, S. P. Reddy and A. B. Malik, *Antioxid. Redox Signaling*, 2014, **20**, 1126–1167.

6 D. R. Green, L. Galluzzi and G. Kroemer, *Science*, 2011, **333**, 1109–1112.
7 T. Bergsbaken, S. L. Fink and B. T. Cookson, *Nat. Rev. Microbiol.*, 2009, **7**, 99.
8 V. Teichgräber, M. Ulrich, N. Endlich, J. Riethmüller, B. Wilker, C. C. De Oliveira–Munding, A. M. Van Heeckeren, M. L. Barr, G. Von Kürthy and K. W. Schmid, *Nat. Med.*, 2008, **14**, 382.
9 A. Mantovani, P. Allavena, A. Sica and F. Balkwill, *Nature*, 2008, **454**, 436.
10 J. Huang, U. M. Upadhyay and R. J. Tamargo, *Surgical Neurology*, 2006, **66**, 232–245.
11 P. Libby, *Am. J. Cardiol.*, 2000, **86**, 3–8.
12 M. De Maat, E. Bladbjerg, T. Drivsholm, K. Borch-Johnsen, L. Møller and J. Jespersen, *J. Thromb. Haemostasis*, 2003, **1**, 950–957.
13 L. Grant, *The Inflammatory Process*, Elsevier, 2nd edn, vol. 2 1973, pp. 205–249.
14 R. M. Zwacka, Y. Zhang, J. Halldorson, H. Schlossberg, L. Dudus and J. F. Engelhardt, *J. Clin. Invest.*, 1997, **100**, 279–289.
15 J. Yang, L. Zhang, C. Yu, X.-F. Yang and H. Wang, *Biomarker Res.*, 2014, **2**, 1.
16 S. J. Galli, S. Nakae and M. Tsai, *Nat. Immunol.*, 2005, **6**, 135.
17 T. C. Theoharides, K.-D. Alysandratos, A. Angelidou, D.-A. Delivanis, N. Sismanopoulos, B. Zhang, S. Asadi, M. Vasiadi, Z. Weng and A. Miniati, *Biochim. Biophys. Acta, Mol. Basis Dis.*, 2012, **1822**, 21–33.
18 M. Cella, A. Engering, V. Pinet, J. Pieters and A. Lanzavecchia, *Nature*, 1997, **388**, 782.
19 M. Kool, T. Soullié, M. van Nimwegen, M. A. Willart, F. Muskens, S. Jung, H. C. Hoogsteden, H. Hammad and B. N. Lambrecht, *J. Exp. Med.*, 2008, **205**, 869–882.
20 A. Chawla, K. D. Nguyen and Y. S. Goh, *Nat. Rev. Immunol.*, 2011, **11**, 738.
21 L. C. Davies, S. J. Jenkins, J. E. Allen and P. R. Taylor, *Nat. Immunol.*, 2013, **14**, 986.
22 J. V. Frangioni, *Curr. Opin. Chem. Biol.*, 2003, **7**, 626–634.
23 E. E. Graves, J. Ripoll, R. Weissleder and V. Ntziachristos, *Med. Phys.*, 2003, **30**, 901–911.
24 J. Chan, S. C. Dodani and C. J. Chang, *Nat. Chem.*, 2012, **4**, 973.
25 L. Yuan, W. Lin, K. Zheng and S. Zhu, *Acc. Chem. Res.*, 2013, **46**, 1462–1473.
26 L. Peng, R. Liu, J. Marik, X. Wang, Y. Takada and K. S. Lam, *Nat. Chem. Biol.*, 2006, **2**, 381.
27 S. Banappagari, A. McCall, K. Fontenot, M. G. H. Vicente, A. Gujar and S. Satyanarayanajois, *Eur. J. Med. Chem.*, 2013, **65**, 60–69.
28 A. Becker, C. Hessenius, K. Licha, B. Ebert, U. Sukowski, W. Semmler, B. Wiedenmann and C. Grötzinger, *Nat. Biotechnol.*, 2001, **19**, 327.
29 Z. Cheng, Y. Wu, Z. Xiong, S. S. Gambhir and X. Chen, *Bioconjugate Chem.*, 2005, **16**, 1433–1441.
30 D. Genovese, E. Rampazzo, S. Bonacchi, M. Montalti, N. Zaccheroni and L. Prodi, *Nanoscale*, 2014, **6**, 3022–3036.
31 S. Santra, B. Liesenfeld, C. Bertolino, D. Dutta, Z. Cao, W. Tan, B. M. Moudgil and R. A. Mericle, *J. Lumin.*, 2006, **117**, 75–82.
32 K. Shimura and B. L. Karger, *Anal. Chem.*, 1994, **66**, 9–15.
33 I. Staub and S. A. Sieber, *J. Am. Chem. Soc.*, 2008, **130**, 13400–13409.
34 N.-Y. Kang, S.-J. Park, X. W. E. Ang, A. Samanta, W. H. P. Driessen, V. Ntziachristos, K. O. Vasquez, J. D. Peterson, S.-W. Yun and Y.-T. Chang, *Chem. Commun.*, 2014, **50**, 6589–6591.
35 R. J. Mellanby, J. I. Scott, I. Mair, A. Fernandez, L. Saul, J. Arlt, M. Moral and M. Vendrell, *Chem. Sci.*, 2018, **9**, 7261–7270.
36 D. Cheng, J. Peng, Y. Lv, D. Su, D. Liu, M. Chen, L. Yuan and X. Zhang, *J. Am. Chem. Soc.*, 2019, **141**, 6352–6361.
37 S. Benson, A. Fernandez, N. D. Barth, F. de Moliner, M. H. Horrocks, S. Herrington, J. L. Abad, A. Delgado, L. Kelly, Z. Chang, Y. Feng, M. Nishiura, Y. Hori, K. Kikuchi and M. Vendrella, *Angew. Chem., Int. Ed.*, 2019, **58**, 6911–6916.
38 Y. Li and T. M. Liu, *Front. Immunol.*, 2018, **9**, 502.
39 A. Fernández and M. Vendrell, *Chem. Soc. Rev.*, 2016, **45**, 1182–1196.
40 A. Vázquez-Romero, N. Kielland, M. J. Arévalo, S. Preciado, R. J. Mellanby, Y. Feng, R. Lavilla and M. Vendrell, *J. Am. Chem. Soc.*, 2013, **135**, 16018–16021.
41 A. Fernandez, M. Vermeren, D. Humphries, R. Subiros-Funosas, N. Barth, L. Campana, A. MacKinnon, Y. Feng and M. Vendrell, *ACS Cent. Sci.*, 2017, **3**, 995–1005.
42 S.-J. Park, B. Kim, S. Choi, S. Balasubramaniam, S.-C. Lee, J. Y. Lee, H. S. Kim, J.-Y. Kim, J.-J. Kim, Y.-A. Lee, N.-Y. Kang, J.-S. Kim and Y.-T. Chang, *Nat. Commun.*, 2019, **10**, 1111.
43 Y. R. Han, S.-H. Shim, D.-S. Kim and C.-H. Jun, *Org. Lett.*, 2017, **19**, 2941–2944.
44 K.-i. Fujita, Y. Takahashi, M. Owaki, K. Yamamoto and R. Yamaguchi, *Org. Lett.*, 2004, **6**, 2785–2788.
45 Z.-W. Chen, Y.-Z. Zhu, J.-W. Ou, Y.-P. Wang and J.-Y. Zheng, *J. Org. Chem.*, 2014, **79**, 10988–10998.
46 M. K. Jha, G. J. Song, M. G. Lee, N. H. Jeoung, Y. Go, R. A. Harris, D. H. Park, H. Kook, I.-K. Lee and K. Suk, *J. Neurosci.*, 2015, **35**, 14353–14369.
47 R. Radhakrishnan, S. A. Moore and K. A. Sluka, *Pain*, 2003, **104**, 567–577.